International Journal of Heat and Mass Transfer 54 (2011) 5286–5297

Contents lists available at SciVerse ScienceDirect

International Journal of Heat and Mass Transfer

journal homepage: www.elsevier.com/locate/ijhmt

Analysis of heat flux bifurcation inside porous media incorporating inertial and dispersion effects – An exact solution

Kun Yang [a], Kambiz Vafai [b,*]

[a] School of Energy and Power Engineering, Huazhong University of Science and Technology, Wuhan 430074, PR China
[b] Department of Mechanical Engineering, University of California, Riverside, CA 92521-0425, USA

ARTICLE INFO

Article history:
Received 24 May 2011
Received in revised form 4 August 2011
Accepted 4 August 2011
Available online 6 September 2011

Keywords:
Heat flux bifurcation
Interface thermal condition
Local Thermal Non-Equilibrium
Thermal dispersion effect
Inertia effect

ABSTRACT

The phenomenon of heat flux bifurcation inside a porous medium is analyzed by studying the convective heat transfer process within a channel partially filled with a porous medium under Local Thermal Non-Equilibrium (LTNE) conditions. Either the thermal dispersion effect or the inertial effect is considered in the physical model. Exact solutions are derived for both the fluid and solid temperature distributions for three interface thermal models at the porous-fluid interface. The required conditions for validity of each interface thermal model are obtained, and the equivalence correlations between different interface thermal models are developed. The range of validity of the Local Thermal Equilibrium (LTE) condition is established, and the phenomenon of heat flux bifurcation inside a porous medium is established and demonstrated for the first time in the literature. Furthermore, the Nusselt number is obtained and investigated for pertinent parameters. The ranges of physical parameters in which the thermal dispersion effect and the inertia effect are important are established.

1. Introduction

LTE and LTNE models are two primary ways for representing heat transfer in a porous medium. LTNE model has gained increased attention in recent years since the assumption of local thermal equilibrium is not valid and the temperature difference between the fluid and solid phases within the porous media are significant in a wide range of applications such as geothermal engineering, heat pipe, electronic cooling, enhanced oil recovery, solar energy utilization and heat transfer enhancement. The internal heat exchange between the fluid and solid phases for LTNE model is complicated under some specified conditions, and will cause the phenomenon of heat flux bifurcation in porous medium. The work of Yang and Vafai [1] was one of the first attempts to study the heat flux bifurcation phenomenon in porous media. They obtained exact solutions for both the fluid and solid temperature distributions for convective heat transfer within a channel filled with a porous medium subject to a constant wall heat flux boundary condition, with internal heat generation in both the fluid and solid phases. They also derived the necessary conditions for temperature gradient bifurcation for the fluid and solid phases at the channel wall. Furthermore, Yang and Vafai [2] demonstrated the existence of two primary types of heat flux bifurcations at the wall under temporal conditions. Heat flux bifurcation in porous media can be considered as a general phenomenon under LTNE condition.

The composite system which consists of a fluid-saturated porous medium and an adjacent fluid layer has received considerable attention due to its wide range of engineering applications. Poulikakos and Kazmierczak [3] studied the forced convection in a duct (parallel plates or circular pipe) partially filled with a porous material. The Brinkman-modified Darcy model was used to model the flow in the porous medium. The results showed that the change of Nusselt number with the thickness of the porous region is not monotonic. Chikh et al. [4] obtained analytical solution of forced convection in an annular duct partially filled a porous medium by using the Brinkman-modified Darcy model. It was found that it may not be necessary to fill the duct completely to attain the maximum heat transfer for highly permeable and conducting material. Alkam et al. [5] numerically investigated the heat transfer enhancement characteristics in the developing region of parallel-plate ducts by attaching a high thermal conductivity porous substrate to the inner wall of one plate. Mohamad [6] numerically investigated the heat transfer in a pipe or a channel by partially inserting the porous materials at the core of the conduit. It was found that the heat transfer can be enhanced with a reasonable pressure drop. Kuznetsov [7] has obtained some solutions for the velocity and temperature distributions for some composite geometrical configurations involving the fluid-porous interface. The LTE model was used in the above-mentioned studies [3–7]. The phenomenon of heat flux bifurcation in porous media was established for the first time in the work of Yang and Vafai [2].

* Corresponding author.
E-mail address: vafai@engr.ucr.edu (K. Vafai).

0017-9310/$ - see front matter © 2011 Elsevier Ltd. All rights reserved.
doi:10.1016/j.ijheatmasstransfer.2011.08.014

Nomenclature

Bi	$Bi = \frac{h_i \alpha H^2}{k_{s,eff}}$, Biot number defined by Eq. (26)
Bi_{int}	$Bi_{int} = \frac{h_{int} H}{k_{s,eff}}$, interface Biot number defined by Eq. (26)
c_p	specific heat of the fluid [J kg^{-1} K^{-1}]
d_p	particle diameter [m]
$D_0, D_1, D_2, D_3, D_4, D_5, D_6, D_7, D_8, D_9$	parameters calculated by Eqs. (51), (63) and (87)
Da	$Da = \frac{K}{H^2}$, Darcy number
F	the geometric function defined by Eq. (8)
h_i	interstitial heat transfer coefficient [W m^{-2} K^{-1}]
h_{int}	interface heat transfer coefficient [W m^{-2} K^{-1}]
h_w	wall heat transfer coefficient defined by Eq. (81) [W m^{-2} K^{-1}]
H	half height of the channel [m]
H_1	half height of the porous media [m]
k	$k = \frac{k_{f,eff}}{k_{s,eff}}$, ratio of the fluid effective thermal conductivity to that of the solid
K	permeability [m^2]
k_0	$k_0 = \frac{k_f}{k_s}$, ratio of the fluid thermal conductivity to that of the solid
k_1	$k_1 = \frac{k_f}{k_{s,eff}}$, ratio of the fluid thermal conductivity to the solid effective thermal conductivity
k_f	thermal conductivity of the fluid [W m^{-1} K^{-1}]
$k_{f,eff}$	effective thermal conductivity of the fluid [W m^{-1} K^{-1}]
k_s	thermal conductivity of the solid [W m^{-1} K^{-1}]
$k_{s,eff}$	effective thermal conductivity of the solid [W m^{-1} K^{-1}]
Nu	Nusselt number
p	pressure [N m^{-2}]
Pr	Prandtl number of fluid
Re_H	$Re_H = -\frac{\rho_f H K}{\mu_f^2}\frac{dp}{dx}$, Reynolds number
Re_p	$Re_p = \frac{\rho_f u_p d_p}{\mu_f}$, particle Reynolds number
q_i	heat flux at the interface [W m^{-2}]
q_w	heat flux at the wall [W m^{-2}]
Q_0	dimensionless internal heat exchange between fluid and solid phases within the region of $0 \leqslant \eta < \eta_0$
Q_1	dimensionless internal heat exchange between fluid and solid phases within the region of $\eta_0 < \eta \leqslant \eta_1$
Q_{int}	dimensionless heat exchange between fluid and solid phases at the interface
T	temperature [K]
u	fluid velocity [m s^{-1}]
u_m	area average velocity over the channel cross section [m s^{-1}]
U	$U = \frac{u}{-\frac{H^2}{\mu_f}\frac{dp}{dx}}$, dimensionless fluid velocity
U_B	dimensionless interface velocity
U_m	dimensionless average velocity over the channel cross section
x	longitudinal coordinate [m]
y	transverse coordinate [m]

Greek symbols

α	interfacial area per unit volume of the porous medium [m^{-1}]
α^*	velocity slip coefficient at the interface
ε	porosity
β	ratio of heat flux for the fluid phase to the total heat flux at the interface
η	$\eta = \frac{y}{H}$, non-dimensional transverse coordinate
η_0	dimensionless transverse location where the dimensionless temperature of fluid is equal to that of solid phase
η_1	$\eta_1 = \frac{H_1}{H}$, non-dimensional half height of the porous media
θ	$\theta = \frac{k_{s,eff}(T - T_{s,i})}{q_w H}$, non-dimensional temperature, defined by Eq. (26)
$\Delta\theta_a$	average relative temperature difference between solid and fluid phases
Λ_H	$\Lambda_H = \frac{F\varepsilon H}{\sqrt{K}}$, inertia parameter
μ	dynamic viscosity [kg m^{-1} s^{-1}]
ρ	density [kg m^{-3}]
γ	$\gamma = \frac{q_i}{q_w}$, dimensionless heat flux at the interface
λ	$\lambda = \sqrt{Bi(1+k)/k}$, parameter calculated by Eq. (49)
ρ	fluid density [kg m^{-3}]

Subscripts

b	bulk mean value
cr	critical value
f	fluid
i	interface
$open$	open region
p	porous region
s	solid phase
w	wall

For the composite systems, the fluid flow and heat transfer boundary conditions at the interface between a porous medium and a fluid have a pronounced effect on the velocity and temperature fields [8–11]. When LTE model is used, the continuity of temperature and heat flux can be utilized as the boundary conditions at the interface. However, since the temperatures of fluid and solid phases are different in porous media for LTNE model, an additional thermal boundary condition should be given at the interface. Jamet and Chandesris [12] discussed the physical nature of the coefficients for jump boundary conditions at fluid-porous interface. d'Hueppe et al. [13] investigated the jump relations at the fluid-porous interface under LTE conditions, and obtained the location of an apparent interface where the condition of continuity is sufficient. To avoid specifying the fluid-porous interface conditions, Aguilar-Madera et al. [14] adopted a one-domain approach to investigate the convective heat transfer in a parallel-plate channel partially filled with a porous medium. Ochoa-Tapia and Whitaker [15] presented the heat flux jump conditions at the interface for LTNE model, in which an excess surface heat transfer coefficient was introduced to control the total heat flux distribution between the solid and fluid phases at the interface. Aguilar-Madera et al. [16] studied the accuracy of the LTE and LTNE models within the inter-region using one-domain approach. Yang and Vafai [17] investigated five of the most fundamental forms of thermal conditions at the interface between a porous medium and a fluid under LTNE condition, and established the restrictions on the validity of each thermal condition. The inertia and thermal dispersion effects become significant in a number of applications such as when dealing with high speed flows and high porosity medium. Vafai and Tien [18] discussed the boundary and inertia effects on flow and heat transfer in porous media. An error map was presented to illustrate the applicability of Darcy's law. Amiri and Vafai [19] presented a comprehensive analysis of the effects of the inertial, boundary, porosity variation and thermal dispersion effects, as well as the validity of local thermal equilibrium assumption in porous media. Jang and Chen [20] numerically investigated the non-Darcy and thermal dispersion effects on the fully developed forced convection parallel plate channel partially filled with a high poros-

ity medium. Jeong and Choi [21] analyzed the thermal dispersion in a porous medium by using the lattice Boltzmann method. Singh et al. [22] analyzed the non-Darcian effects on natural convection flow in a vertical channel partially filled with a porous medium. Alkam et al. [5] and Mohamad [6] also discussed the influence of inertia effects in porous media.

The present study aims at revealing the phenomenon of heat flux bifurcation inside a composite system under LTNE conditions, by adopting both the thermal dispersion effect and the inertia effect. Three porous-fluid interface thermal models are utilized in the present study. The analytical solutions for the fluid and solid phase temperature distributions and the Nusselt number are obtained. The influence of the pertinent parameters such as Darcy number, particle Reynolds number, inertia parameter, Biot number, and interface Biot number are discussed to compare the physical features.

2. Modeling and formulation

Fig. 1 shows the configurations under consideration, in which fluid flows through a rectangular channel partially filled with a porous medium in the core region, and subject to a constant heat, q_w. The height of the channel is $2H$, and that of the porous medium is $2H_1$. We assume constant fluid properties. The velocity and temperature profiles are considered to be fully developed, and the momentum equation for porous region is represented by the Darcian–Forchheimer model.

Based on these assumptions, the governing conservation equations for the porous region are obtained from the works of Amiri and Vafai [19] based on the LTNE model.

Fluid phase

$$k_{f,eff}\frac{\partial^2 T_f}{\partial y^2}+h_i\alpha(T_s-T_f)=\rho c_p u\frac{\partial T_f}{\partial x} \tag{1}$$

Solid phase

$$k_{s,eff}\frac{\partial^2 T_s}{\partial y^2}-h_i\alpha(T_s-T_f)=0 \tag{2}$$

where T_f and T_s denote the fluid and solid temperatures, $k_{f,eff}$ and $k_{s,eff}$ the effective fluid and solid thermal conductivities, u the fluid velocity, ρ the density of the fluid, c_p the specific heat of the fluid, h_i the interstitial heat transfer coefficient, and α is the interfacial area per unit volume of the porous medium.

The effective thermal conductivities of both phases are obtained as

$$k_{f,eff}=\varepsilon k_f \tag{3}$$

$$k_{s,eff}=(1-\varepsilon)k_s \tag{4}$$

where k_f and k_s are the fluid and solid thermal conductivities, respectively, and ε denotes the porosity.

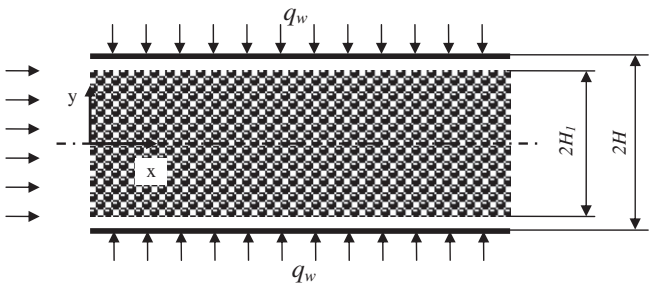

Fig. 1. Schematic diagram of the physical model and the corresponding coordinate system.

When the thermal dispersion effect is accounted for, the effective thermal conductivities of fluid phases is represented as [19]

$$k_{f,eff}=(\varepsilon+0.1\mathrm{Pr}Re_p)k_f \tag{5}$$

where Pr denotes the Prandtl number of fluid, Re_p the particle Reynolds number,

$$Re_p=\frac{\rho_f u_p d_p}{\mu_f} \tag{6}$$

where d_p denotes particle diameter and u_p is the velocity in the porous medium.

The momentum equation in the porous region can be written as

$$-\frac{\mu_f}{K}u-\frac{\rho_f F\varepsilon}{\sqrt{K}}u^2-\frac{dp}{dx}=0 \tag{7}$$

where K denotes the permeability, μ_f the fluid dynamic viscosity, p the pressure and F the geometric function. Parameter F is obtained as [19]

$$F=\frac{1.75}{\sqrt{150\varepsilon^3}} \tag{8}$$

The momentum and energy equations in the open region are

$$-\frac{dp}{dx}+\mu_f\frac{d^2u}{dy^2}=0 \tag{9}$$

$$k_f\frac{\partial^2 T_f}{\partial y^2}=\rho c_p u\frac{\partial T_f}{\partial x} \tag{10}$$

The boundary conditions at the wall and the interface are

$$\left.\frac{\partial u}{\partial y}\right|_{y=0}=0 \tag{11}$$

$$\left.\frac{\partial T_f}{\partial y}\right|_{y=0}=\left.\frac{\partial T_s}{\partial y}\right|_{y=0}=0 \tag{12}$$

$$u|_{y=H}=0 \tag{13}$$

$$\left.k_f\frac{\partial T_f}{\partial y}\right|_{y=H}=q_w \tag{14}$$

$$\left.\frac{\partial u}{\partial y}\right|_{y=H_1^+}=\frac{\alpha^*}{\sqrt{K}}(u_B-u_p) \tag{15}$$

where u_B denotes the interface velocity and α^* the velocity slip coefficient, and the slip velocity condition at the interface between the open and porous regions based on Beavers and Joseph [8] model is adopted here.

In this work, we utilize three models to describe the thermal interface conditions at the fluid-porous interface. These are Models A, B and C.

2.1. Model A

If the heat transfer between fluid and solid phases at the interface is very substantial, then the temperatures of both phases can be considered to be equal. This constitutes Model A. That is

$$T_f|_{y=H_1^-}=T_s|_{y=H_1^-}=T_f|_{y=H_1^+} \tag{16}$$

$$\left.k_{f,eff}\frac{\partial T_f}{\partial y}\right|_{y=H_1^-}+\left.k_{s,eff}\frac{\partial T_s}{\partial y}\right|_{y=H_1^-}=\left.k_f\frac{\partial T_f}{\partial y}\right|_{y=H_1^+}=q_i \tag{17}$$

where q_i is the total heat flux at the interface.

2.2. Model B

When the heat transfer between the fluid and solid phases at the interface is not strong enough, the fluid and solid temperatures at the interface will not be equal. As such, the total heat flux distribution between the solid and fluid phases at the interface is evaluated by an interface thermal parameter, β. This is the basis for Model B.

$$T_f|_{y=H_1^-} = T_f|_{y=H_1^+} \tag{18}$$

$$k_f \frac{\partial T_f}{\partial y}\bigg|_{y=H_1^+} = q_i \tag{19}$$

$$k_{f,eff} \frac{\partial T_f}{\partial y}\bigg|_{y=H_1^-} = \beta q_i \tag{20}$$

$$k_{s,eff} \frac{\partial T_s}{\partial y}\bigg|_{y=H_1^-} = (1-\beta) q_i \tag{21}$$

where β is the ratio of heat flux for the fluid phase to the total heat flux at the interface.

2.3. Model C

The temperatures of fluid and solid phases are also not equal at the interface for Model C, and the heat exchange between fluid and solid phases at the interface is calculated by introducing an interface heat transfer coefficient, h_{int}, based on the heat flux jump interfacial condition developed by Ochoa-Tapia and Whitaker [15]

$$T_f|_{y=H_1^-} = T_f|_{y=H_1^+} \tag{22}$$

$$k_f \frac{\partial T_f}{\partial y}\bigg|_{y=H_1^+} = q_i \tag{23}$$

$$k_{f,eff} \frac{\partial T_f}{\partial y}\bigg|_{y=H_1^-} = q_i - h_{int}\left(T_f|_{y=H_1^-} - T_s|_{y=H_1^-}\right) \tag{24}$$

$$k_{s,eff} \frac{\partial T_s}{\partial y}\bigg|_{y=H_1^-} = h_{int}\left(T_f|_{y=H_1^-} - T_s|_{y=H_1^-}\right) \tag{25}$$

where h_{int} is the interface heat transfer coefficient.

The following non-dimensional variables have been introduced

$$\begin{gathered}\theta = \frac{k_{s,eff}(T-T_{s,i})}{q_w H} \quad \eta = \frac{y}{H} \quad \eta_1 = \frac{H_1}{H} \quad \gamma = \frac{q_i}{q_w} \\ k_0 = \frac{k_f}{k_s} \quad k = \frac{k_{f,eff}}{k_{s,eff}} \quad k_1 = \frac{k_f}{k_{s,eff}} \quad Bi = \frac{h_i \alpha H^2}{k_{s,eff}} \quad Bi_{int} = \frac{h_{int} H}{k_{s,eff}} \\ Da = \frac{K}{H^2} \quad U = \frac{u}{-\frac{H^2}{\mu_f}\frac{dp}{dx}} \quad \Lambda_H = \frac{F\varepsilon H}{\sqrt{K}} \quad Re_H = -\frac{\rho_f H K}{\mu_f^2}\frac{dp}{dx}\end{gathered} \tag{26}$$

where $T_{s,i}$ is the temperature of solid phase at the interface.

Adding governing Eqs. (1) and (2), the following equation is obtained

$$k_{f,eff}\frac{\partial^2 T_f}{\partial y^2} + k_{s,eff}\frac{\partial^2 T_s}{\partial y^2} = \rho c_p u \frac{\partial T_f}{\partial x} \tag{27}$$

Integrating Eq. (27) from the center to the fluid-porous interface and applying the corresponding boundary Eq. (12) and interface Eq. (17) for Model A, or Eqs. (20) and (21) for Model B, or Eqs. (24) and (25) for Model C, result in

$$\rho c_p u_p \frac{\partial T_f}{\partial x} = \frac{q_i}{H_1} \tag{28}$$

A similar equation is obtained by integrating the energy Eq. (10) in open region from the interface to the wall and using the corresponding boundary and interface conditions.

$$\rho c_p u_{m,open} \frac{\partial T_f}{\partial x} = \frac{q_w - q_i}{H - H_1} \tag{29}$$

where $u_{m,open}$ is the average fluid velocity in the open region.

Based on the momentum Eqs. (7) and (9) and the corresponding boundary and interface conditions (11), (13) and (15), the velocity distributions are obtained as

In the porous region:

$$U = U_p \quad 0 \leqslant \eta \leqslant \eta_1 \tag{30}$$

where U_p denotes the dimensionless velocity in porous medium.

$$U_p = \frac{-1 + \sqrt{1 + 4Da\Lambda_H Re_H}}{2\Lambda_H Re_H} \tag{31}$$

In the open region:

$$U = -0.5(\eta - \eta_1)^2 + \frac{\alpha^*}{\sqrt{Da}}(U_B - U_p)(\eta - \eta_1) + U_B \quad \eta_1 < \eta \leqslant 1 \tag{32}$$

where U_B is the dimensionless interface velocity

$$U_B = \frac{0.5(1-\eta_1)^2 + \frac{\alpha^*}{\sqrt{Da}}U_p(1-\eta_1)}{1 + \frac{\alpha^*}{\sqrt{Da}}(1-\eta_1)} \tag{33}$$

Based on Eq. (32), the dimensionless average velocity in the open region is obtained as

$$U_{m,open} = -\frac{1}{6}(1-\eta_1)^2 + \frac{\alpha^*}{2\sqrt{Da}}(U_B - U_p)(1-\eta_1) + U_B \tag{34}$$

Based on Eqs. (31) and (34), the dimensionless average velocity over the channel cross section is obtained as

$$U_m = \eta_1 U_p + (1-\eta_1) U_{m,open} \tag{35}$$

Based on Eqs. (28), (29), (30), (34) and (35), the dimensionless total heat flux at the interface is obtained as

$$\gamma = \frac{q_i}{q_w} = \frac{\eta_1 U_p}{U_m} \tag{36}$$

2.4. Temperature solution for interface thermal condition of Model A

The energy governing equations and the corresponding boundary and interface conditions for Model A are normalized by using Eqs. (26) and (30)–(36)

$$k\frac{\partial^2 \theta_f}{\partial \eta^2} + Bi(\theta_s - \theta_f) = \frac{\gamma}{\eta_1} \quad 0 \leqslant \eta \leqslant \eta_1 \tag{37}$$

$$\frac{\partial^2 \theta_s}{\partial \eta^2} - Bi(\theta_s - \theta_f) = 0 \quad 0 \leqslant \eta \leqslant \eta_1 \tag{38}$$

$$k_1 \frac{\partial^2 \theta_f}{\partial \eta^2} = \frac{U}{U_m} \quad \eta_1 < \eta \leqslant 1 \tag{39}$$

$$\frac{\partial \theta_f}{\partial \eta}\bigg|_{\eta=0} = \frac{\partial \theta_s}{\partial \eta}\bigg|_{\eta=0} = 0 \tag{40}$$

$$\theta_f|_{\eta=\eta_1^-} = \theta_s|_{\eta=\eta_1^-} = \theta_f|_{\eta=\eta_1^+} = 0 \tag{41}$$

$$\frac{\partial \theta_f}{\partial \eta}\bigg|_{\eta=1} = \frac{1}{k_1} \tag{42}$$

Based on Eqs. (37) and (38), the governing equations for fluid and solid phases in the porous region are obtained as

$$k\theta_f'''' - (1+k)Bi\theta_f'' = -Bi\frac{\gamma}{\eta_1} \tag{43}$$

$$k\theta_s'''' - (1+k)Bi\theta_s'' = -Bi\frac{\gamma}{\eta_1} \tag{44}$$

Differentiating Eqs. (37) and (38) and utilizing the boundary and interface conditions (40) and (41), the following equations are obtained.

$$\theta_f''(\eta_1^-) = \frac{\gamma}{\eta_1 k} \quad \theta_s''(\eta_1^-) = 0 \tag{45}$$

$$\theta_f'''(0) = \theta_s'''(0) = 0 \tag{46}$$

Solving Eqs. (43) and (44) and applying the boundary equations (40), (41), (45) and (46), the temperature distribution in the porous region is obtained as

$$\theta_f = \frac{\gamma}{(1+k)\eta_1}\left\{\frac{1}{2}(\eta^2-\eta_1^2) + \frac{1}{(1+k)Bi}\left[\frac{\cosh(\lambda\eta)}{\cosh(\lambda\eta_1)} - 1\right]\right\} \tag{47}$$

$$\theta_s = \frac{\gamma}{(1+k)\eta_1}\left\{\frac{1}{2}(\eta^2-\eta_1^2) + \frac{k}{(1+k)Bi}\left[1 - \frac{\cosh(\lambda\eta)}{\cosh(\lambda\eta_1)}\right]\right\} \tag{48}$$

where,

$$\lambda = \sqrt{Bi(1+k)/k} \tag{49}$$

Solving Eq. (39) and applying the boundary Eqs. (41) and (42), the temperature distribution in the open region is obtained as

$$\theta_f = D_0(\eta-\eta_1)^4 + D_1(\eta-\eta_1)^3 + D_2(\eta-\eta_1)^2 + D_3(\eta-\eta_1) \tag{50}$$

where

$$\begin{aligned} D_0 &= -\frac{1}{24U_m k_1} \\ D_1 &= \frac{\alpha^*}{6U_m k_1\sqrt{Da}}(U_B - U_p) \\ D_2 &= \frac{U_B}{2U_m k_1} \\ D_3 &= \frac{1}{k_1} - 4D_0(1-\eta_1)^3 - 3D_1(1-\eta_1)^2 - 2D_2(1-\eta_1) \end{aligned} \tag{51}$$

2.5. Temperature solution for interface thermal condition of Model B

The interface thermal conditions for Model B are normalized as

$$\theta_s|_{\eta=\eta_1^-} = 0 \tag{52}$$

$$\left.\frac{\partial\theta_f}{\partial\eta}\right|_{\eta=\eta_1^-} = \frac{\beta\gamma}{k} \tag{53}$$

$$\theta_f|_{\eta=\eta_1^-} = \theta_f|_{\eta=\eta_1^+} \tag{54}$$

Solving governing Eqs. (37)–(39) and applying the boundary and interface condition Eqs. (40), (42), (52), (53) and (54), the temperature distributions are obtained as

In the porous region

$$\theta_f = \frac{\gamma}{(1+k)\lambda\sinh(\lambda\eta_1)}[\beta - k(1-\beta)]\left[\frac{\cosh(\lambda\eta)}{k} + \cosh(\lambda\eta_1)\right] + \frac{\gamma(\eta^2-\eta_1^2)}{2\eta_1(1+k)} - \frac{\gamma}{(1+k)\eta_1 Bi} \tag{55}$$

$$\theta_s = \frac{\gamma}{(1+k)\lambda\sinh(\lambda\eta_1)}[\beta - k(1-\beta)][\cosh(\lambda\eta_1) - \cosh(\lambda\eta)] + \frac{\gamma(\eta^2-\eta_1^2)}{2\eta_1(1+k)} \tag{56}$$

In the open region

$$\theta_f = D_0(\eta-\eta_1)^4 + D_1(\eta-\eta_1)^3 + D_2(\eta-\eta_1)^2 + D_3(\eta-\eta_1) + \theta_f(\eta_1^-) \tag{57}$$

where $\theta_f(\eta_1^-)$ is calculated using equation (55), D_0, D_1, D_2 and D_3 are calculated using Eq. (51).

2.6. Temperature solution for interface thermal condition of Model C

The interface thermal conditions for Model C are normalized as

$$\theta_s|_{\eta=\eta_1^-} = 0 \tag{58}$$

$$k\left.\frac{\partial\theta_f}{\partial\eta}\right|_{\eta=\eta_1^-} = \gamma - Bi_{int}\left(\theta_f|_{\eta=\eta_1^-} - \theta_s|_{\eta=\eta_1^-}\right) \tag{59}$$

$$\theta_f|_{\eta=\eta_1^-} = \theta_f|_{\eta=\eta_1^+} \tag{60}$$

Solving governing Eqs. (37)–(39) and applying the boundary and interface condition Eqs. (40), (42), (58), (59) and (60), the temperature solutions are obtained as

In porous region

$$\theta_f = \frac{\gamma D_4}{\lambda^2\eta_1}\cosh(\lambda\eta) + \frac{\gamma\eta^2}{2\eta_1(1+k)} + \gamma\eta_1 D_5 \tag{61}$$

$$\theta_s = \frac{\gamma D_6}{\lambda^2\eta_1}\cosh(\lambda\eta) + \frac{\gamma\eta^2}{2\eta_1(1+k)} + \gamma\eta_1 D_7 \tag{62}$$

where

$$\begin{aligned} D_4 &= \frac{Bi\eta_1 + Bi_{int}}{\lambda k^2\sinh(\lambda\eta_1) + Bi_{int}k(1+k)\cosh(\lambda\eta_1)} \\ D_5 &= \frac{D_4 k^2}{Bi\eta_1^2(1+k)}\cosh(\lambda\eta_1) - \frac{1}{Bi\eta_1^2(1+k)} - \frac{1}{2(1+k)} \\ D_6 &= \frac{D_8 Bi_{int}\eta_1(1+k) - 1}{\sinh(\lambda\eta_1)(1+k)}\lambda\eta_1 \\ D_7 &= -\frac{D_6}{\lambda^2\eta_1^2}\cosh(\lambda\eta_1) - \frac{1}{2(1+k)} \\ D_8 &= \frac{D_4}{\lambda^2\eta_1^2}\cosh(\lambda\eta_1) + \frac{1}{2(1+k)} + D_5 \end{aligned} \tag{63}$$

In open region

$$\theta_f = D_0(\eta-\eta_1)^4 + D_1(\eta-\eta_1)^3 + D_2(\eta-\eta_1)^2 + D_3(\eta-\eta_1) + \theta_f(\eta_1^-) \tag{64}$$

where $\theta_f(\eta_1^-)$ is calculated using equation (61), D_0, D_1, D_2 and D_3 are calculated using Eq. (51).

3. Results and discussion

3.1. Validity of the interface thermal models

The dimensionless fluid phase temperature should be larger than the dimensionless solid phase temperature at the interface based on the second law of thermodynamics. That is

$$\theta_f|_{\eta=\eta_1^-} \geqslant \theta_s|_{\eta=\eta_1^-} \tag{65}$$

Also, the dimensionless temperature gradient of the solid phase at the interface should larger than zero. That is

$$\left.\frac{\partial\theta_s}{\partial\eta}\right|_{\eta=\eta_1^-} \geqslant 0 \tag{66}$$

Substituting Eqs. (61) and (62) in Eqs. (65) and (66), results in

$$Bi_{int} \geqslant 0 \tag{67}$$

Substituting Eqs. (55) and (56) in Eqs. (65) and (66), results in

$$1 \geqslant \beta \geqslant \beta_{cr} \tag{68}$$

where, β_{cr} denotes critical ratio of heat flux for the fluid phase to the total heat flux at the interface. Based on equation (68), β_{cr} stands for the minimum ratio of heat flux for the fluid phase to the total heat flux at the interface. Based on equations (20) and (21), the maximum ratio of heat flux for the solid phase to the total heat flux at the interface is equal to $1-\beta_{cr}$.

$$\beta_{cr} = \frac{\frac{\sinh(\lambda\eta_1)}{\lambda\eta_1\cosh(\lambda\eta_1)} + k}{1+k} \tag{69}$$

The distributions of critical heat flux ratio β_{cr} for different parameters Bi, k_0 and Re_p are shown in Fig. 2. It is found from Eq. (69) that β_{cr} increases as k becomes larger. or η_1 and Bi become smaller. Therefore, when the thermal dispersion effect is excluded, β_{cr} increases as k_0 becomes larger since k increases with k_0, as shown in Fig. 2(a). When the thermal dispersion effect is incorporated, β_{cr} increases as Re_p becomes larger since k increases with Re_p, as shown in Fig. 2(b). When k is large and Bi is small, β_{cr} will increases up to about 1, which means most of the total heat flux at the interface should be transferred into porous region through the fluid phase.

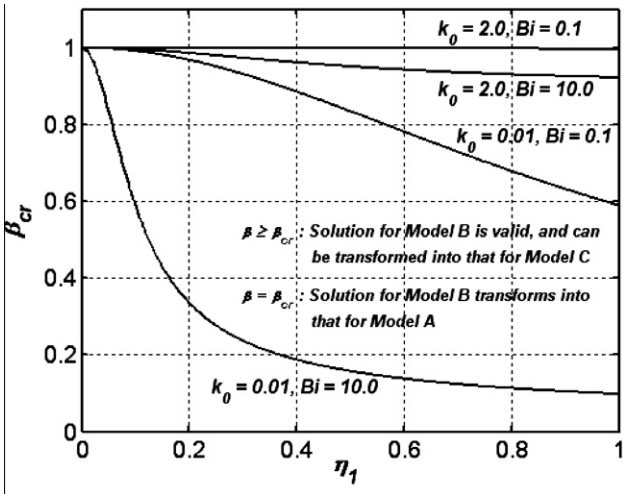

(a) thermal dispersion effects excluded

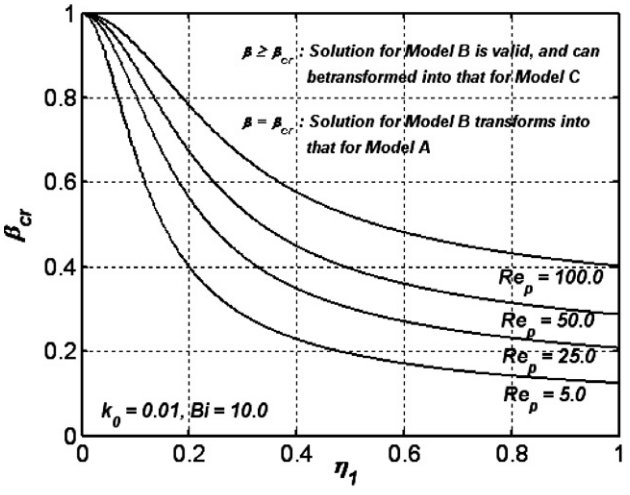

(b) thermal dispersion effects incorporated

Fig. 2. β_{cr} distributions for pertinent parameters Bi, k_0 and Re_p for $\varepsilon = 0.8$.

3.2. Equivalence correlations between each interface thermal model

An important physical feature is found by comparing the temperature solutions for different interface thermal models. These solutions become equivalent to each other under the following conditions:

(a) When $\beta = \beta_{cr}$, the temperatures of fluid and solid phases at the interface are equal, thus the solution for Model B is equivalent to that for Model A.
(b) When $\beta = 1 - D_8 Bi_{int}\eta_1$, the solution for Model B is equivalent to that for Model C.
(c) When $Bi_{int} \to \infty$, the temperatures of fluid and solid phases at the interface are equal, thus the solution for Model C is equivalent to that for Model A.
(d) When $Bi_{int} \to 0$, there is no heat exchange between fluid and solid phases at the interface, thus the solution for Model C is equivalent to that for Model B for $\beta = 1$.

3.3. Temperature distributions and heat flux bifurcation phenomenon

Fig. 3 shows the dimensionless temperature distributions as a function of η_1, k_0, β, Re_p, Λ_H and Bi. When $\Lambda_H = 0$, the inertia effect is excluded, otherwise, the inertia effect is incorporated. The temperature difference between the fluid and the channel wall is found to decreases while the inertia and the thermal dispersion effects are incorporated. This temperature difference also decreases when Re_p and Bi increases. When Bi is small, which translates into a weak internal heat transfer between the fluid and solid phases, the temperature difference between the two phases is relatively large. However, when η_1 is small, the temperature difference between the two phases is quite small, even for a small Bi, as shown in Fig. 3(c). This is because, when η_1 is small, the total heat flux at the interface is also small, as shown in Fig. 4. Since only a small amount of heat flux will be transferred through the porous region, the influence of Bi can be negligible. Fig. 4 displays the variations of total heat flux at the interface as a function of pertinent parameters Λ_H, Re_p and Da. It is found that the total heat flux at the interface decreases while the inertia effect is incorporated, and decreases as Re_p becomes larger or Da and η_1 becomes smaller. However, when Da is smaller than 10^{-5}, the influence of Re_p and Λ_H can be neglected. When η_1 is smaller than 0.4, the heat flux transferred into the porous region is so insignificant that the influence of Re_p and Λ_H can be neglected. Furthermore, it can be found from Eq. (36) that, when the inertia effect is excluded, the total heat flux at the interface is independent of Re_p.

It is important to note that the direction of heat exchange between the fluid and solid phases are different in two regions inside the porous medium, as shown in Fig. 3(a) and (b). This leads to a heat flux bifurcation for those cases. The condition for this phenomenon can be derived as

$$1 \geqslant \beta > \beta_{cr} \tag{70}$$

Based on the equivalence correlation between Model B and Model C, Eq. (70) can be rewritten as

$$0 \leqslant Bi_{int} < \infty \tag{71}$$

Eq. (71) shows that, when the interface heat transfer coefficient does not approach infinity, the phenomenon of heat flux bifurcation

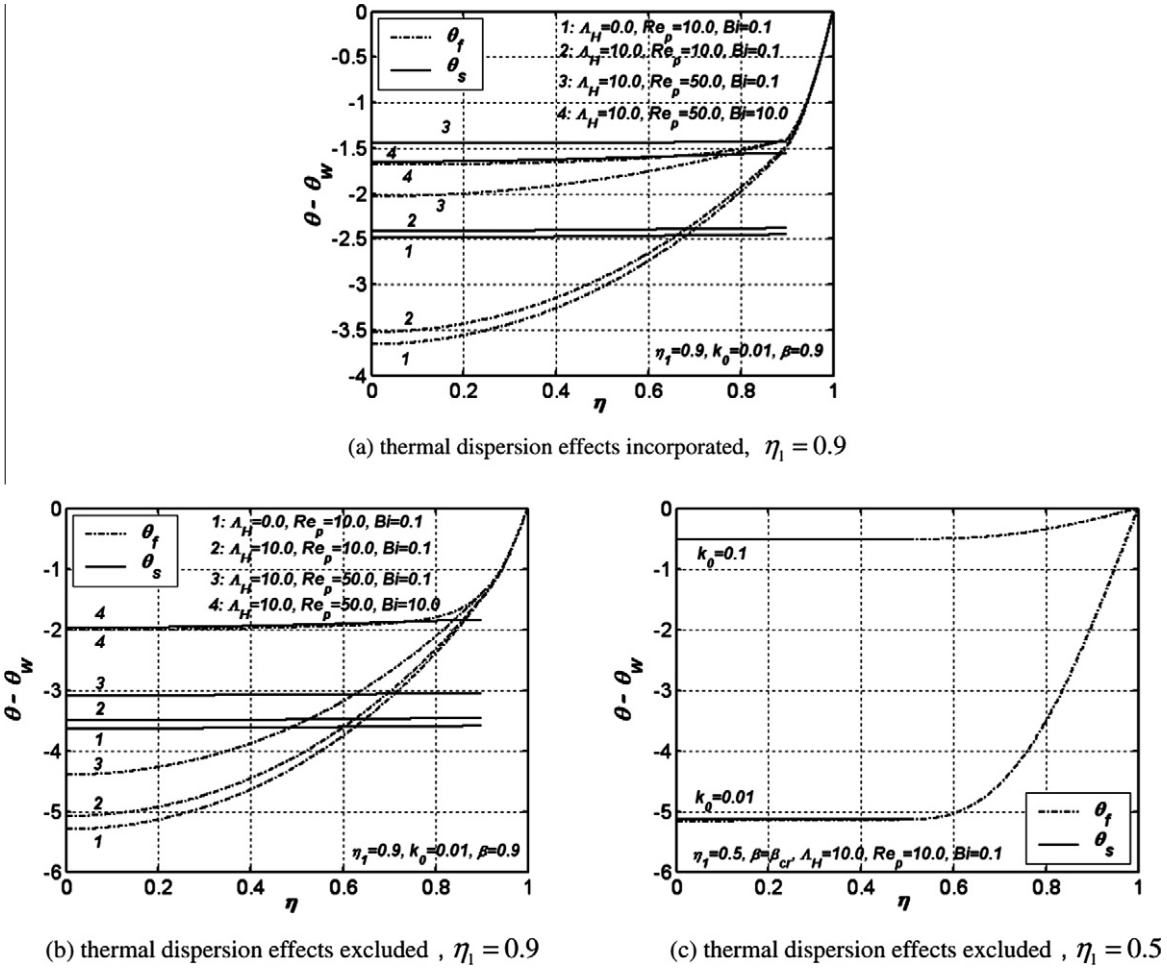

(a) thermal dispersion effects incorporated, $\eta_1 = 0.9$

(b) thermal dispersion effects excluded , $\eta_1 = 0.9$

(c) thermal dispersion effects excluded , $\eta_1 = 0.5$

Fig. 3. Dimensionless temperature distributions for Model B for $\alpha^* = 0.78$, $Da = 1 \times 10^{-4}$ and $\varepsilon = 0.8$.

will occur inside the two regions, $0 \leqslant \eta < \eta_0$ and $\eta_0 < \eta \leqslant \eta_1$. Within the region of $\eta_0 < \eta \leqslant \eta_1$, the dimensionless temperature of fluid phase is larger than that of the solid phase, while within the region of $0 \leqslant \eta < \eta_0$, the dimensionless temperature of fluid phase is smaller than that of the solid phase. The value of η_0 can be obtained by setting the temperatures of fluid and solid phases to be equal. Based on equations (55) and (56), it is found that

$$\eta_0 = \frac{1}{\lambda}\ \mathrm{acosh}\left\{\frac{\sinh(\lambda\eta_1)}{\lambda\eta_1[\beta - k(1-\beta)]}\right\} \tag{72}$$

It is found from Eq. (72) that η_0 increases as β becomes smaller. When β approaches β_{cr}, η_0 will approach η_1. The distributions of η_0 for pertinent parameters Bi, k_0 and Re_p are shown in Fig. 5. When the thermal dispersion effect is excluded and $\beta = 1$, η_0 increases as k_0 becomes smaller or Bi becomes larger, as shown in Fig. 5(a). When the thermal dispersion effect is incorporated and $\beta = 1$,η_0 increases as Re_p becomes smaller, as shown in Fig. 5(b).

The dimensionless internal heat exchange between fluid and solid phases within the region of $0 \leqslant \eta < \eta_0$ is obtained as

$$Q_0 = \int_0^{\eta_0} Bi(\theta_f - \theta_s)d\eta = \frac{\gamma}{1+k}\left\{[\beta - k(1-\beta)]\frac{\sinh(\lambda\eta_0)}{\sinh(\lambda\eta_1)} - \frac{\eta_0}{\eta_1}\right\} \tag{73}$$

The dimensionless internal heat exchange between fluid and solid phases within the region of $\eta_0 < \eta \leqslant \eta_1$ is obtained as

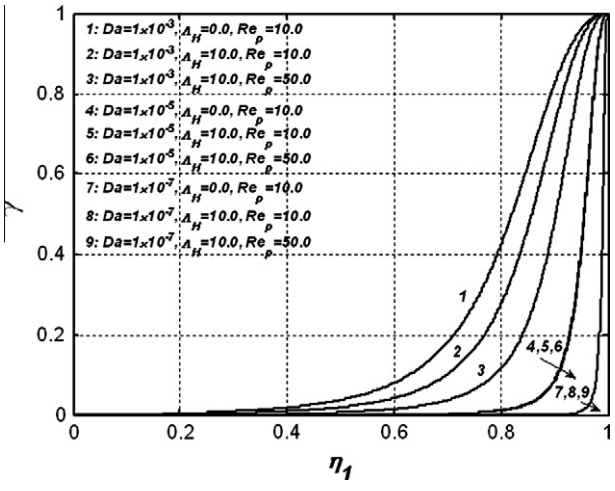

Fig. 4. Dimensionless total heat flux distributions at the interface for $\alpha^* = 0.78$.

$$Q_1 = \int_{\eta_0}^{\eta_1} Bi(\theta_f - \theta_s)d\eta = \frac{\gamma}{1+k}\left\{[\beta - k(1-\beta)]\left(1 - \frac{\sinh(\lambda\eta_0)}{\sinh(\lambda\eta_1)}\right) - \left(1 - \frac{\eta_0}{\eta_1}\right)\right\} \tag{74}$$

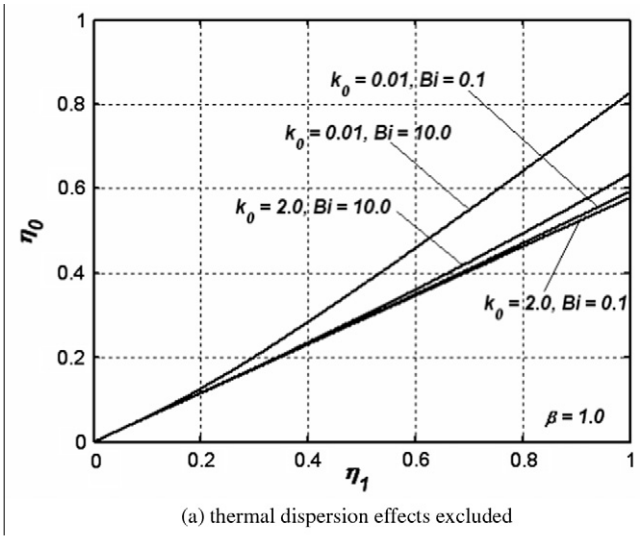

(a) thermal dispersion effects excluded

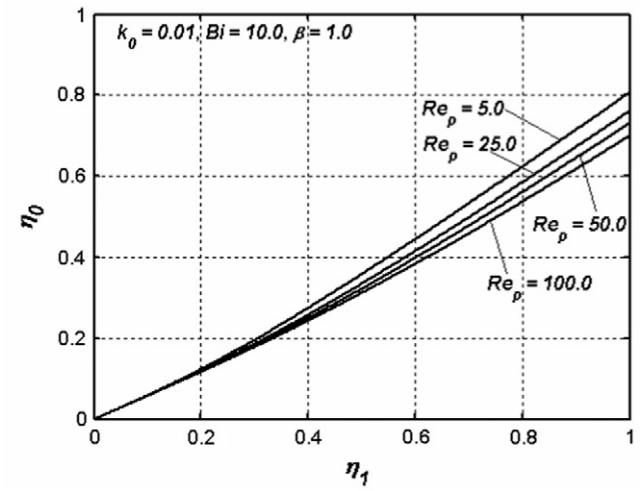

(b) thermal dispersion effects incorporated

Fig. 5. η_0 distributions for pertinent parameters Bi, k_0 and Re_p for $\varepsilon = 0.8$.

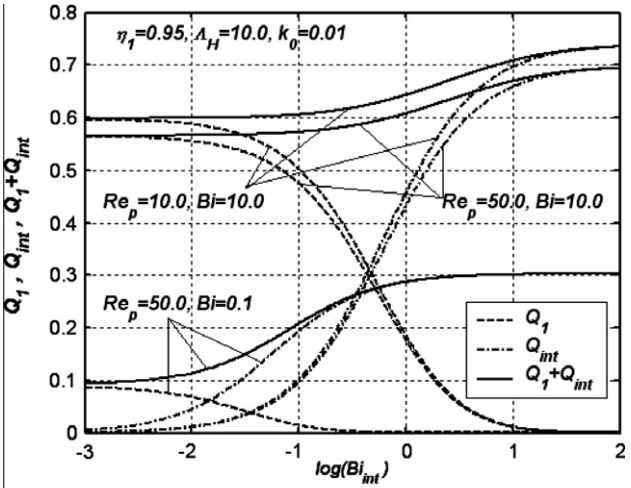

(a) thermal dispersion effects excluded

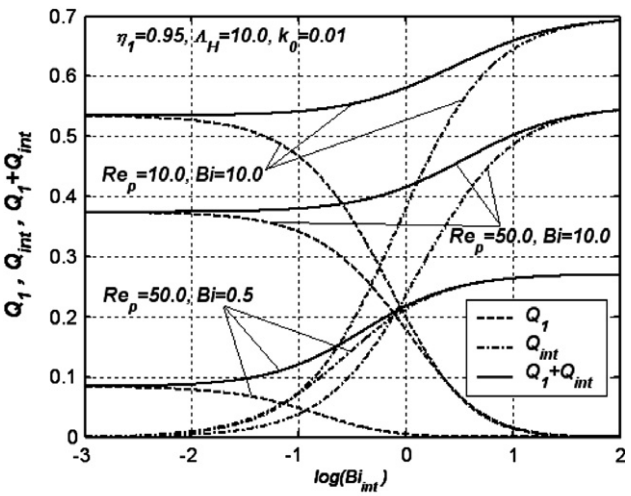

(b) thermal dispersion effects incorporated

Fig. 6. Q_1, Q_{int}, and $Q_1 + Q_{int}$ distributions for pertinent parameters Re_p, Bi and Bi_{int} for $\alpha^* = 0.78$, $Da = 1 \times 10^{-4}$ and $\varepsilon = 0.8$.

The dimensionless heat exchange between fluid and solid phases at the interface is obtained as

$$Q_{int} = Bi_{int}(\theta_f - \theta_s)_{\eta=\eta_1} = (1-\beta)\gamma \tag{75}$$

Based on Eqs. (74)–(76), the following equation is obtained

$$Q_0 + Q_1 + Q_{int} = 0 \tag{76}$$

It should be noted that Q_1 and Q_{int} are always equal to or larger than zero, and Q_0 is always equal to or less than zero. $Q_1 + Q_{int}$ represents the total heat energy transferred from the fluid to the solid phase within the region of $\eta_0 < \eta \leqslant \eta_1$ and interface, which will be transferred back to fluid phase within the region of $0 \leqslant \eta < \eta_0$ based on Eq. (76). The distributions of Q_1, Q_{int}, and $Q_1 + Q_{int}$ for pertinent parameters Re_p, Bi and Bi_{int} are shown in Fig. 6. It is found that Bi and Bi_{int} are the major parameters that affect Q_1 and Q_{int}. Q_1 decreases with Bi_{int}, and Q_{int} and $Q_1 + Q_{int}$ increase with Bi_{int}. The figure also shows that, when the heat flux bifurcation occurs, the total heat energy transferred from the fluid to the solid phase within the region of $\eta_0 < \eta \leqslant \eta_1$ and interface will decrease. When Bi_{int} is small, Q_1 is larger than Q_{int}; when Bi_{int} is large, Q_{int} is larger than Q_1. When Bi_{int} approaches zero, Q_1 will approach a maximum value and Q_{int} will approach zero. However, when Bi_{int} approaches infinity, Q_1 will approach zero, and Q_{int} and $Q_1 + Q_{int}$ will approach a maximum value. When Bi_{int} is very small or large, the variations of Q_1, Q_{int} and $Q_1 + Q_{int}$ with Bi_{int} are negligible. However, for intermediate values of Bi_{int}, the variations of Q_1, Q_{int} and $Q_1 + Q_{int}$ with Bi_{int} are quite substantial. It can also be seen that Q_1, Q_{int}, and $Q_1 + Q_{int}$ increase as Re_p becomes smaller, or for larger values of Bi.

3.4. LTE condition

The average relative temperature difference between solid and fluid phases within the porous region is calculated as follows:

$$\Delta\theta_a = \frac{\int_0^{\eta_1} |\theta_f - \theta_s| d\eta}{(\theta_f|_{\eta=1} - \theta_f|_{\eta=0})\eta_1} = \frac{Q_1 - Q_0}{(\theta_f|_{\eta=1} - \theta_f|_{\eta=0})Bi_i\eta_1} \tag{77}$$

It should be noted that, because of the occurrence of the heat flux bifurcation phenomenon, the average relative temperature difference between solid and fluid phases within the porous region can not be calculated as follow:

$$\Delta\theta_{a\_1} = \frac{\int_0^{\eta_1} (\theta_f - \theta_s) d\eta}{(\theta_f|_{\eta=1} - \theta_f|_{\eta=0})\eta_1} = \frac{Q_1 + Q_0}{(\theta_f|_{\eta=1} - \theta_f|_{\eta=0})B_i\eta_1} = \frac{-Q_{int}}{(\theta_f|_{\eta=1} - \theta_f|_{\eta=0})B_i\eta_1} \tag{78}$$

Otherwise, when Bi_{int} approaches zero, Q_{int} will approach zero, thus the average relative temperature difference calculated according to Eq. (78) will approach zero, which is obviously unreasonable.

When $\Delta\theta_a$ is small enough, the LTE condition is considered to be valid. In this work, the criterion for LTE condition is chosen to be $\Delta\theta_a < 2\%$. Based on Eq. (77), $\Delta\theta_a$ is found to decrease as η_1 becomes smaller. Therefore, a critical $\eta_{1,cr}$ can be introduced to examine the LTE condition. That is.

(a) when $\eta_1 > \eta_{1,cr}$, $\Delta\theta_a > 2.0\%$, thus the LTE condition is considered to be invalid;
(b) when $\eta_1 < \eta_{1,cr}$, $\Delta\theta_a < 2.0\%$, thus the LTE condition is considered to be valid,

where, $\eta_{1,cr}$ is determined based on the following equation

$$\Delta\theta_a|_{\eta_1=\eta_{1,cr}} = 2.0\% \tag{79}$$

The $\eta_{1,cr}$ variations as a function of pertinent parameters Bi, Bi_{int}, Re_p, Λ_H and Da are shown in Figs. 7 and 8. It is found that $\eta_{1,cr}$ increases as Da becomes smaller, or Re_p become larger, or the inertia effect is incorporated, which is the result of the decrease in the total heat flux transferred into the porous region, as shown in Fig. 4. It is also found that $\eta_{1,cr}$ increases as Bi becomes larger, since a larger Bi can be translated into a strong internal heat transfer between the fluid and solid phases. However, when η_1 is small enough, the LTE condition is valid, even for a small Bi. This is because the total heat flux transferred into the porous region decreases as η_1 becomes smaller, as shown in Fig. 4. Comparing between Fig. 7(a) and (b), it is found that, when the thermal dispersion effect is incorporated, $\eta_{1,cr}$ will increase, which also can be seen in Fig. 8. This is because the dispersion phenomenon is treated as an additional diffusive term for the effective conductivity of fluid phase based on Eq. (5) [19]. Fig. 8 reveals that Bi_{int} has a complicated influence on the $\eta_{1,cr}$ distributions. When Bi is small, $\eta_{1,cr}$ will increase as Bi_{int} becomes smaller. However, when Bi is large, $\eta_{1,cr}$ will reach its maximum value at moderate values of Bi_{int}.

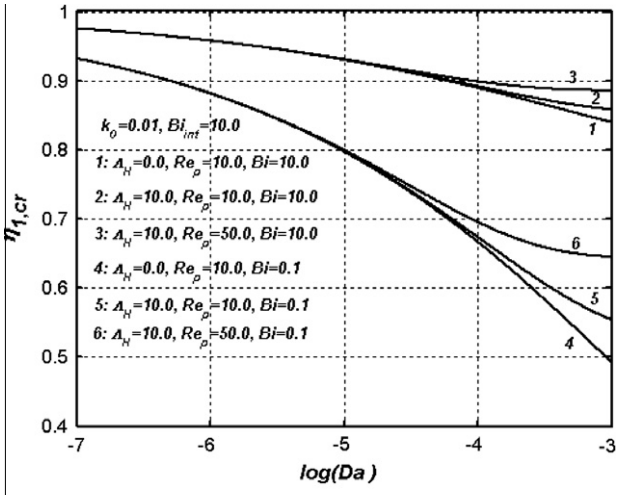

(a) thermal dispersion effects excluded

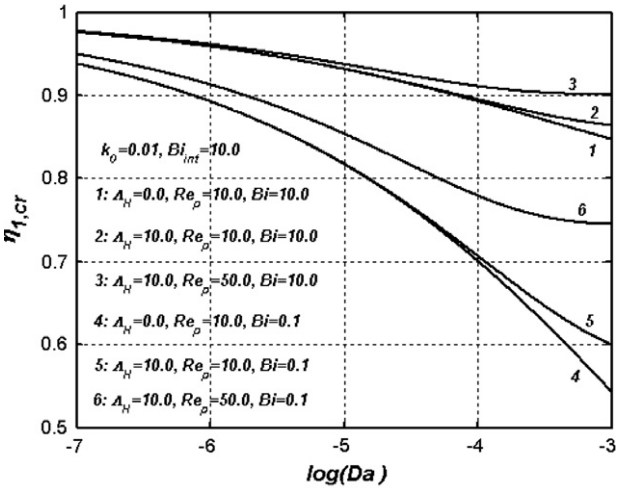

(b) thermal dispersion effects incorporated

Fig. 7. $\eta_{1,cr}$ variations as a function of Da for $\alpha^* = 0.78$ and $\varepsilon = 0.8$.

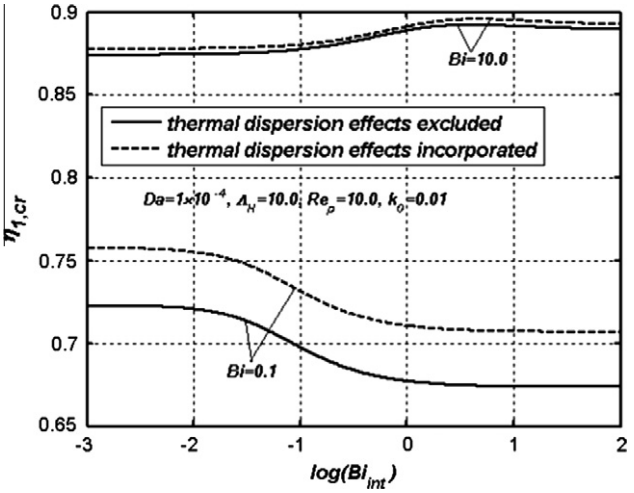

Fig. 8. $\eta_{1,cr}$ variations as a function of Bi_{int} for $\alpha^* = 0.78$ and $\varepsilon = 0.8$.

3.5. Nusselt number results

The non-dimensional bulk mean temperature of the fluid can be calculated as

$$\theta_{f,b} = \frac{\int_0^1 \theta_f(\eta) U d\eta}{U_m} \tag{80}$$

The wall heat transfer coefficient is defined by

$$h_w = \frac{q_w}{T_{f,w} - T_{f,b}} \tag{81}$$

and the Nusselt number can be presented as

$$Nu = \frac{h_w(4H)}{k_f} = \frac{4}{k_1(\theta_{f,w} - \theta_{f,b})} \tag{82}$$

where $4H$ is the hydraulic diameter of the channel.

Nusselt number for interface thermal condition of Model B can be obtained by substituting Eqs. (30), (32), (55) and (57) in Eqs. (80) and (82). These results in

$$Nu = \frac{h_w(4H)}{k_f} = \frac{4}{k_1\left[D_0(1-\eta_1)^4 + D_1(1-\eta_1)^3 + D_2(1-\eta_1)^2 + D_3(1-\eta_1) + \theta_f(\eta_1^-) - \theta_{f,b}\right]} \tag{83}$$

where

$$\theta_{f,b} = \frac{\theta_{f,pm} U_p \eta_1 + \theta_{f,om} U_{m,open}(1-\eta_1)}{U_m} \tag{84}$$

$$\theta_{f,pm} = \frac{\gamma}{(1+k)\lambda\sinh(\lambda\eta_1)}[\beta - k(1-\beta)]\left[\frac{\sinh(\lambda\eta_1)}{\lambda\eta_1 k} + \cosh(\lambda\eta_1)\right] - \frac{\gamma\eta_1}{3(1+k)} - \frac{\gamma}{(1+k)\eta_1 Bi} \tag{85}$$

$$\theta_{f,om} = \frac{1}{U_{m,open}}\left[-\frac{D_0}{14}(1-\eta_1)^6 + \left(\frac{-0.5D_1 + D_0D_9}{6}\right)(1-\eta_1)^5 + \left(\frac{-0.5D_2 + D_1D_9 + U_BD_0}{5}\right)(1-\eta_1)^4 + \left(\frac{-0.5D_3 + D_2D_9 + U_BD_1}{4}\right)(1-\eta_1)^3 + \left(\frac{-0.5\theta_f(\eta_1^-) + D_3D_9 + U_BD_2}{3}\right)(1-\eta_1)^2 + \left(\frac{\theta_f(\eta_1^-)D_9 + U_BD_3}{2}\right)(1-\eta_1) + \theta_f(\eta_1^-)U_B\right] \tag{86}$$

$$D_9 = \frac{\alpha^*}{\sqrt{Da}}(U_B - U_p) \tag{87}$$

The Nusselt number for interface thermal conditions of Models A and C can be obtained by substituting the corresponding equivalence correlations, $\beta = \beta_{cr}$ and $\beta = 1 - D_8 Bi_{int}\eta_1$ in Eqs. (83)–(86), respectively.

The Nusselt number variations as a function of pertinent parameters Bi, Bi_{int}, Re_p, Λ_H and Da are shown in Fig. 9. It is found that the Nusselt number increases while the thermal dispersion effect is incorporated. This is because the effective conductivity of fluid phase increases with the inclusion of the thermal dispersion effect. When all the other parameters are unchanged, the Nusselt number will increase while the inertia effect is incorporated. This is because, when Re_p is unchanged, the total fluid mass flow over the channel cross section will increase with the inclusion of the inertia effect. In most cases, the Nusselt number will increase as Re_p becomes larger. However, when both the thermal dispersion effect and the inertia effect are excluded, the Nusselt number is independent of Re_p. When all the other parameters are maintained unchanged, the total fluid mass flow over the channel cross section will increase as Da becomes smaller. This results in an enhancement in the Nusselt number, as shown in Fig. 9(b). When Bi or Bi_{int} increases, the heat transfer between fluid and solid phases is enhanced inside the porous region or at the interface, thus the Nusselt number will increase, as shown in Fig. 9(b). When η_1 is small, the total heat flux transferred into the porous region is also small, thus the influences of Bi, Bi_{int}, Re_p, Λ_H and Da on the Nusselt numbers become weak, as shown in Fig. 9(a) and (b).

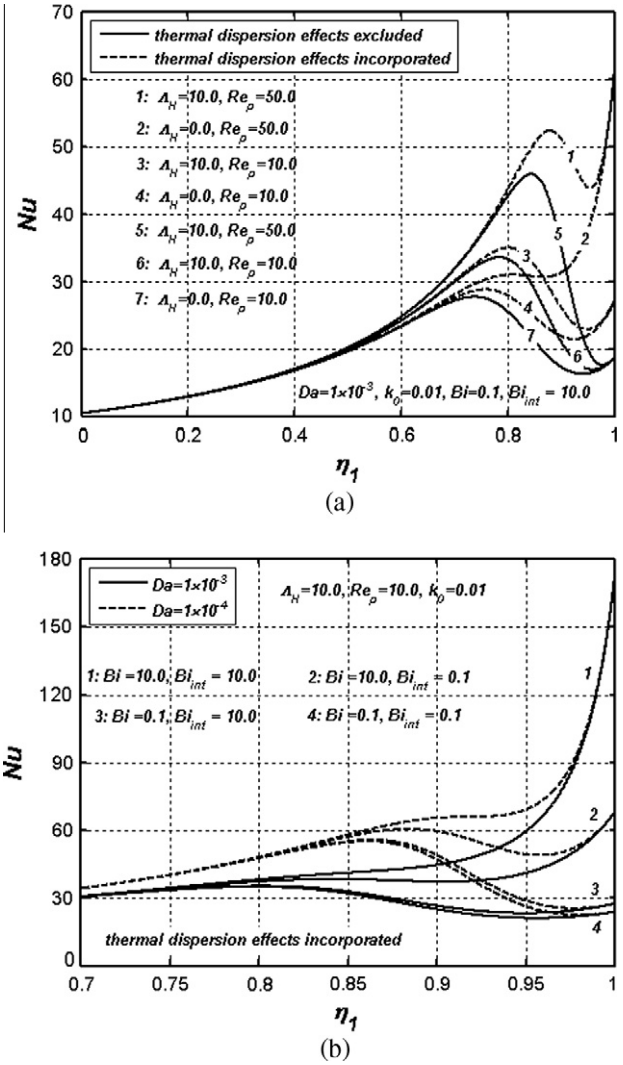

Fig. 9. Nusselt number variations as a function of pertinent parameters Bi, Bi_{int}, Re_p, Λ_H and Da for $\alpha^* = 0.78$ and $\varepsilon = 0.8$.

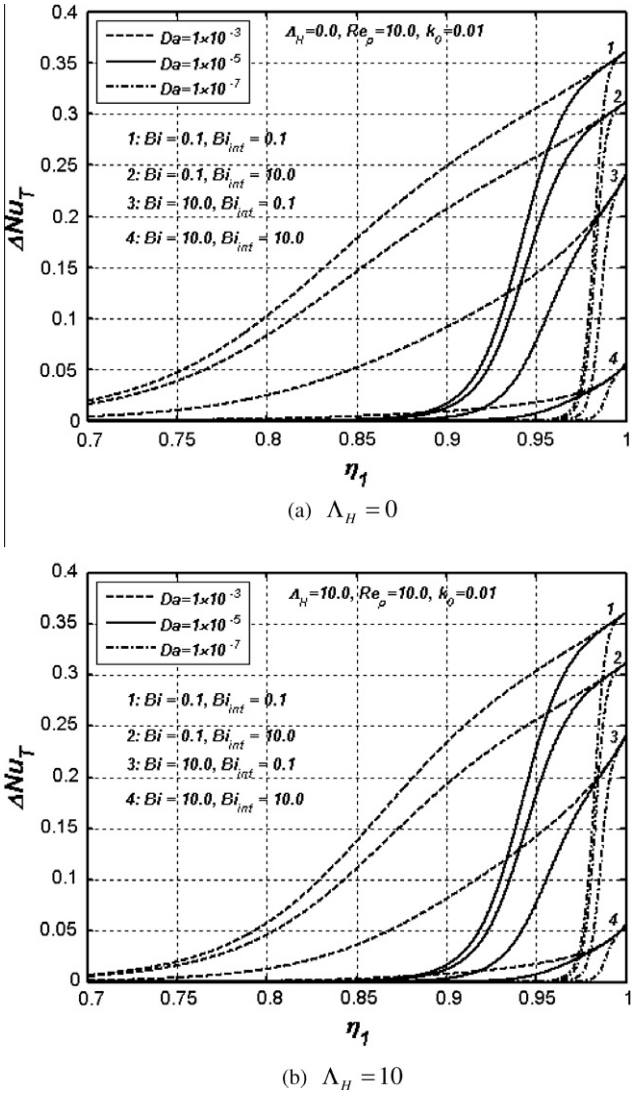

Fig. 10. ΔNu_T distributions for pertinent parameters Bi, Bi_{int}, Re_p, Λ_H and Da for $\alpha^* = 0.78$ and $\varepsilon = 0.8$.

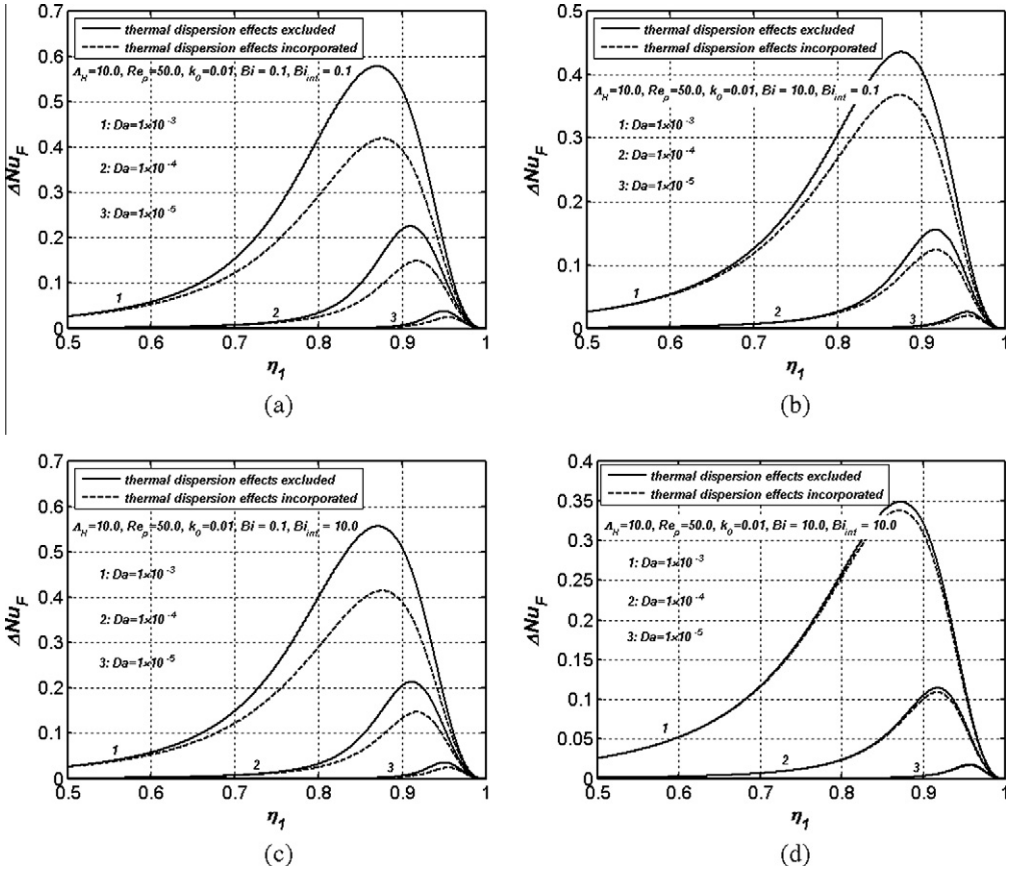

Fig. 11. ΔNu_F distributions for pertinent parameters Bi, Bi_{int}, Re_p, Λ_H and Da for $\alpha^* = 0.78$ and $\varepsilon = 0.8$.

3.6. Thermal dispersion effect and inertia effect

To further investigate the significance of the thermal dispersion effect, the difference between the Nusselt numbers obtained from including and ignoring the thermal dispersion effect is calculated. That is

$$\Delta Nu_T = \frac{Nu_T - Nu_{NT}}{Nu_T} \tag{88}$$

where Nu_T is the Nusselt number adopting the thermal dispersion effect, while Nu_{NT} is the Nusselt number when the thermal dispersion effect is neglected.

To further investigate the significance of the inertia effect, the difference between the Nusselt numbers obtained from adopting the inertia effect or neglecting it is calculated. That is

$$\Delta Nu_F = \frac{Nu_F - Nu_{NF}}{Nu_F} \tag{89}$$

where Nu_F is the Nusselt number which incorporates the inertia effect, while Nu_{NF} is the Nusselt number based on neglecting the inertia effect.

ΔNu_T distributions reflecting the influence of pertinent parameters Bi, Bi_{int}, Re_p, Λ_H and Da are shown in Fig. 10. As mentioned earlier, ΔNu_T decreases as η_1 becomes smaller. It is found that Da plays a major role on the distribution of ΔNu_T. When Da becomes smaller, ΔNu_T will decrease, and approaches zero at smaller values of η_1. When η_1 approaches unit, the velocity distribution becomes uniform, thus ΔNu_T for different Da values will approach the same value. When Bi or Bi_{int} increases, ΔNu_T will decrease, which means that the influence of the thermal dispersion effect becomes weaker as the heat exchange between the fluid and solid phases is enhanced. By comparing Fig. 10(a) and (b), it can be seen that the thermal dispersion effect becomes less significant when the inertia effect is incorporated.

ΔNu_F distributions incorporating the influence of pertinent parameters Bi, Bi_{int}, Re_p, Λ_H and Da are shown in Fig. 11. It can be seen that ΔNu_F approaches zero as η_1 becomes smaller or when η_1 approaches unity. As such the inertial effects are more pronounced for moderate values of η_1. It can also be seen that Da plays a major role on the distribution of ΔNu_F. When Da is less than 10^{-5}, the inertial effect can be neglected. When Bi or Bi_{int} increases, ΔNu_F will decrease, since the influence of the inertial effect become weaker as the heat exchange between the fluid and solid phases is enhanced. It is also found that the inertia effect become weaker when the thermal dispersion effect is incorporated.

4. Conclusions

The phenomenon of heat flux bifurcation inside a porous medium is analyzed in this work. To this end, convective heat transfer within a channel partially filled with a porous medium under LTNE model, with consideration of both the thermal dispersion and inertial effects, is investigated analytically. Exact solutions are derived for the fluid and solid temperature distributions and Nusselt number for three interface thermal models at the porous-fluid interface. The range of validity of all the interface thermal models is established in this work. The equivalence correlations between different interface thermal models are developed. When the heat transfer between the fluid and solid phases does not approach infinity, and the temperatures are not equal at the porous-fluid interface, the phenomenon of heat flux bifurcation will occur inside the porous media. The average temperature difference between the fluid and solid phases inside the porous media, in which the phenomenon of heat flux bifurcation should be consid-

ered, is used to determine the LTE condition. The results show that a critical dimensionless half height of the porous media is a proper parameter, below which the LTE condition within porous region is considered to be valid. Furthermore, the Darcy number and the dimensionless half height of the porous media are the two major parameters which influence the thermal dispersion effect and the inertial effect. It is also found that the thermal dispersion effect becomes weaker when the inertial effect is incorporated, and the inertial effect becomes weaker when the thermal dispersion effect is incorporated.

References

[1] K. Yang, K. Vafai, Analysis of temperature gradient bifurcation in porous media – An exact solution, Int. J. Heat Mass Transfer 53 (2010) 4316–4325.

[2] K. Yang, K. Vafai, Transient aspects of heat flux bifurcation in porous media: an exact solution, ASME J. Heat Transfer 133 (2011) 052602.

[3] D. Poulikakos, M. Kazmierczak, Forced convection in a duct partially filled with a porous material, ASME J. Heat Transfer 109 (1987) 653–662.

[4] S. Chikh, A. Boumedien, K. Bouhadef, G. Lauriat, Analytical solution of non-Darcian forced convection in an annular duct partially filled with a porous medium, Int. J. Heat Mass Transfer 38 (9) (1995) 1543–1551.

[5] M.K. Alkam, M.A. Al-Nimr, M.O. Hamdan, Enhancing heat transfer in parallel-plate channels by using porous inserts, Int. J. Heat Mass Transfer 44 (2001) 931–938.

[6] A.A. Mohamad, Heat transfer enhancements in heat exchangers fitted with porous media Part I: constant wall temperature, Int. J. Therm. Sci. 42 (4) (2003) 385–395.

[7] A.V. Kuznetsov, Analytical Studies of Forced Convection in Partly Porous Configurations, in: K. Vafai (Ed.), Handbook of Porous Media, Dekker, New York, 2000, pp. 269–315.

[8] G.S. Beavers, D.D. Joseph, Boundary conditions at a naturally permeable wall, J. Fluid Mech. 30 (1) (1967) 197–207.

[9] K. Vafai, R. Thiyagaraja, Analysis of flow and heat transfer at the interface region of a porous medium, Int. J. Heat Mass Transfer 30 (1987) 1391–1405.

[10] K. Vafai, S. Kim, Fluid mechanics of the interface region between a porous medium and a fluid layer – an exact solution, Int. J. Heat Fluid Flow 11 (1990) 254–256.

[11] B. Alazmi, K. Vafai, Analysis of fluid flow and heat transfer interfacial conditions between a porous medium and a fluid layer, Int. J. Heat Mass Transfer 44 (2001) 1735–1749.

[12] D. Jamet, M. Chandesris, On the intrinsic nature of jump coefficients at the interface between a porous medium and a free fluid region, Int. J. Heat Mass Transfer 52 (1–2) (2009) 289–300.

[13] A. d'Hueppe, M. Chandesris, D. Jamet, B. Goyeau, Boundary conditions at a fluid-porous interface for a convective heat transfer problem: analysis of the jump relations, Int. J. Heat Mass Transfer 54 (15–16) (2011) 3683–3693.

[14] Carlos G. Aguilar-Madera, Francisco J. Valdés-Parada, Benoît Goyeau, J. Alberto Ochoa-Tapia, Convective heat transfer in a channel partially filled with a porous medium, Int. J. Therm. Sci. 50 (8) (2011) 1355–1368.

[15] J.A. Ochoa-Tapia, S. Whitaker, Heat transfer at the boundary between a porous medium and a homogeneous fluid, Int. J. Heat Mass Transfer 40 (11) (1997) 2691–2707.

[16] Carlos G. Aguilar-Madera, Francisco J. Valdés-Parada, Benoît Goyeau, J. Alberto Ochoa-Tapia, One-domain approach for heat transfer between a porous medium and a fluid, Int. J. Heat Mass Transfer 54 (9-10) (2011) 2089–2099.

[17] K. Yang, K. Vafai, Restrictions on the validity of the thermal conditions at the porous-fluid interface – an exact solution, ASME J. Heat Transfer, in press.

[18] K. Vafai, C.L. Tien, Boundary and inertia effects on flow and heat transfer in porous media, Int. J. Heat Mass Transfer 24 (1981) 195–203.

[19] A. Amiri, K. Vafai, Analysis of dispersion effects and non-thermal equilibrium non-Darcian, variable porosity incompressible flow through porous medium, Int. J. Heat Mass Transfer 37 (1994) 939–954.

[20] J.Y. Jang, J. L Chen, Forced convection in a parallel plate channel partially filled with a high porosity medium, Int. Com. Heat Mass Transfer 19 (1992) 263–273.

[21] N. Jeong, D.H. Choi, Estimation of the thermal dispersion in a porous medium of complex structures using a lattice Boltzmann method, Int. J. Heat Mass Transfer 54 (2011) 4389–4399.

[22] Atul Kumar Singh, Pratibha Agnihotri, N.P. Singh, Ajay Kumar Singh, Transient and non-Darcian effects on natural convection flow in a vertical channel partially filled with porous medium: analysis with Forchheimer–Brinkman extended Darcy model, Int. J. Heat Mass Transfer 54 (5–6) (2011) 1111–1150.